Inorganic Chemistry
Article

Inorg. Chem. **2011**, *50*, 1021–1029 **1021**
DOI: 10.1021/ic101691q

Experimental and Theoretical Mössbauer Study of an Extended Family of $[Fe_8(\mu_4\text{-}O)_4(\mu\text{-}4\text{-}R\text{-}px)_{12}X_4]$ Clusters

Ekaterina M. Zueva,[†] W. M. C. Sameera,[‡] Dalice M. Piñero,[§] Indranil Chakraborty,[§] Eamonn Devlin,[⊥] Peter Baran,[§,¶] Katarina Lebruskova,[§] Yiannis Sanakis,[*,⊥] John E. McGrady,[*,‡] and Raphael G. Raptis[*,§]

[†]*Department of Inorganic Chemistry, Kazan State Technological University, Kazan, K. Marx 68, 420015, Russia,* [‡]*Inorganic Chemistry Laboratory, Department of Chemistry, University of Oxford, South Parks Road, Oxford, OX1 3QR, United Kingdom,* [§]*Department of Chemistry and the Institute for Functional Nanomaterials, University of Puerto Rico, San Juan, Puerto Rico 00936-8377, United States, and* [⊥]*Institute of Materials Science, NCRS "Demokritos", 15310 Aghia Paraskevi, Athens, Greece.* [¶] *Present address: Department of Chemistry, Juniata College, Huntingdon, PA, 16652, United States.*

Received August 19, 2010

Six $[Fe_8(\mu_4\text{-}O)_4(\mu\text{-}4\text{-}R\text{-}pyrazolato)_{12}X_4]$ complexes containing an identical $Fe_8(\mu_4\text{-}O)_4$ core have been structurally characterized and studied by Mössbauer spectroscopy. In each case, an inner μ_4-O bridged Fe^{III} cubane core is surrounded by four trigonal bipyramidal iron centers, the two distinct sites occurring in a 1:1 ratio. The Mössbauer spectrum of each of the clusters consists of two quadrupole doublets, which, with one exception (X = NCS, R = H), overlap to give three absorption lines. The systematic variation of X and R causes significant changes in the Mössbauer spectra. A comparison with values for the same clusters computed using density functional theory allows us to establish an unequivocal assignment of these peaks in terms of a nested model for the overlapping doublets. The changes in Mössbauer parameters (both experimental and computed) for the 1-electron reduced species $[Fe_8(\mu_4\text{-}O)_4(\mu\text{-}4\text{-}Cl\text{-}pyrazolato)_{12}Cl_4]^-$ are consistent with a redox event that is localized within the cubane core.

Introduction

Multinuclear metal clusters, most notably the di-, tri-, and tetranuclear Fe/S-clusters of the ferredoxins, play a central role in biological electron transfer.[1] Their biological function depends on the ability of these clusters to accept and release electrons reversibly, and so the redox characteristics, which are determined by both the intrinsic properties of the metal clusters and the protein and solvent environment, are of paramount importance.[2] Holm and co-workers have characterized several redox-modified $[Fe_4S_4\text{-}(SR)_4]$* species, which model the analogous active centers of ferredoxins.[2a,3] Many of the accessible redox states of these Fe_4 clusters are mixed valent, containing Fe^{II} and Fe^{III} species, and the nature of this mixed valency has been investigated extensively: localized and delocalized (either fully or partially) systems are known.[4] Mössbauer spectroscopy has played an important part in the study of mixed valency in these iron systems, as it can distinguish redox-inequivalent sites on a typical time scale of 10^{-8} s. For example, the Mössbauer spectrum of the $[4Fe\text{-}4S]^{3+}$ active center of HiPIP(oxidized) from *C. vinosum* consists of two quadrupole doublets of equal intensity whose isomer shifts differ by ~0.06 mm/s, assigned to one $Fe^{3+}-Fe^{3+}$ and one delocalized $Fe^{2.5+}-Fe^{2.5+}$ pair.[5] Similar behavior has been also noted for the model complex, $[Fe_4S_4(S\text{-}2,4,6\text{-}i\text{-}Pr_3C_6H_2)_4]^-$.[6] In contrast, the $[4Fe\text{-}4S]^{2+}$ active center of HiPIP(reduced) from *B. stearothermophilus*, as well as two of its model complexes, $[Fe_4S_4(SPh)_4]^{2-}$ and $[Fe_4S_4\text{-}(SCH_2Ph)_4]^{2-}$, exhibits only a single doublet, indicating complete delocalization (four $Fe^{2.5+}$ centers with isomer shift

*To whom correspondence should be addressed. E-mail: sanakis@ims.demokritos.gr (Y.S.); john.mcgrady@chem.ox.ac.uk (J.E.M.); raphael@epscor.upr.edu (R.G.R.).

(1) (a) Johnson, D. C.; Dean, D. R.; Smith, A. D.; Johnson, M. K. *Annu. Rev. Biochem.* **2005**, *74*, 247. (b) Beinert, H. *J. Biol. Inorg. Chem.* **2000**, *5*, 2.
(2) (a) Rao, P. V.; Holm, R. H. *Chem. Rev.* **2004**, *104*, 527. (b) Dey, A.; Jenney, F. E.; Adams, M. W. W.; Babini, E.; Takahashi, Y.; Fukuyama, K.; Hodgson, K. O.; Hedman, B.; Solomon, E. I. *Science* **2007**, *318*, 1464. (c) Saridakis, E.; Giastas, P.; Efthymiou, G.; Thoma, V.; Moulis, J.-M.; Kyritsis, P.; Mavridis, I. M. *J. Biol. Inorg. Chem.* **2009**, *14*, 783.
(3) (a) Scott, T. A.; Berlinguette, C. P.; Holm, R. H.; Zhou, H.-C. *Proc. Natl. Acad. Sci.* **2005**, *102*, 9741. (b) Deng, L.; Holm, R. H. *J. Am. Chem. Soc.* **2008**, *130*, 9878.
(4) (a) Marks, A. J. *J. Chem. Phys.* **2008**, *129*, 054311and references therein. (b) Papaefthymiou, V.; Girerd, J. J.; Moura, I.; Moura, J. J. G.; Münck, E. *J. Am. Chem. Soc.* **1987**, *109*, 4703. (c) Achim, C.; Bominaar, E.; Meyer, J.; Peterson, J.; Münck, E. *J. Am. Chem. Soc.* **1999**, *121*, 3704. (d) Achim, C.; Bominaar, E.; Staples, R. J.; Münck, E.; Holm, R. H. *Inorg. Chem.* **2001**, *40*, 4389. (e) Bominaar, E.; Achim, C.; Borshch, S. A.; Girerd, J.-J.; Münck, E. *Inorg. Chem.* **1997**, *36*, 3689.
(5) Middleton, P.; Dickson, D. P. E.; Johnson, C. E.; Rush, J. D. *Eur. J. Biochem.* **1980**, *104*, 289.
(6) Papaefthymiou, V.; Millar, M. M.; Münck, E. *Inorg. Chem.* **1986**, *25*, 3010.

Published on Web 12/28/2010

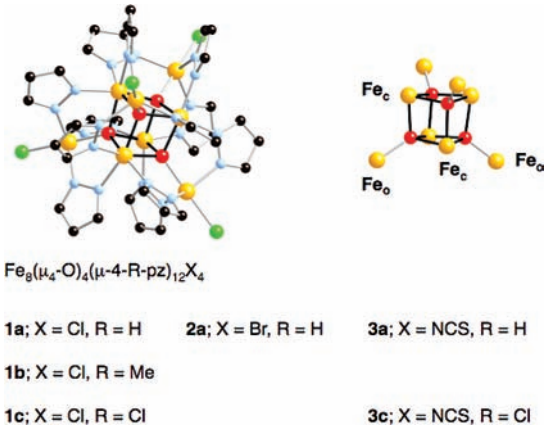

Figure 1. Ball-and-stick diagram of the Fe_8 cluster and its $Fe_8(\mu_4\text{-}O)_4$-core denoting the outer and cubane Fe sites: yellow, Fe; red, O; blue, N; green, X.

of ~0.4 mm/s). For the $[4Fe\text{-}4S]^{1+}$ center of Fd(reduced) from *B. stearothermophilus* (and the corresponding model complexes, $[Fe_4S_4(SCH_2Ph)_4]^{3-}$ and $[Fe_4S_4(SPh)_4]^{3-}$),[7] the Mössbauer spectrum shows two quadrupole doublets of almost equal intensity assigned to one $Fe^{2+}-Fe^{2+}$ and one $Fe^{2.5+}-Fe^{2.5+}$ pair.

In contrast to the iron−sulfur proteins that are ubiquitous in nature, iron-oxo analogues appear not to have such a prominent role in biological electron transfer reactions, despite the fact that iron oxide mineral sources are abundant. Thus, although several metalloproteins with dinuclear Fe/O active centers are known,[8] higher nuclearity Fe/O-clusters are rare. A tetranuclear Fe_4O_4 cluster has been identified in a protein isolated from the blood of a mollusk, although its structure remains uncertain; cubane or "Jacob's ladder" structures have been proposed.[9] Recently, an octanuclear Fe^{III}-oxo cluster with a μ_{eff} value approximating the value previously determined by some of us for a $[Fe_8(\mu_4\text{-}O)_4(\mu\text{-}pz)_{12}Cl_4]$ compound has been proposed as the unit exiting the oxireductase site of ferritin and subsequently being added to its ferrihydrite cluster core.[10] The intriguing possibility that Fe_4O_4 or Fe_4O_8 cores may have a previously unsuspected biological role has motivated us to study a family of octanuclear $[Fe_8(\mu_4\text{-}O)_4(\mu\text{-}4\text{-}R\text{-}pz)_{12}X_4]$ (Fe_8) clusters which contain a Fe_8O_4 core supported by pyrazole ligands bridging the cubane to four outer Fe^{III} centers (Figure 1).[11] The outer irons (Fe_o) have a trigonal bipyramidal coordination sphere composed of three nitrogens from bridging pyrazolates in the equatorial positions and one axial terminal ligand (a chloride in the complex shown in Figure 1) *trans* to a μ_4-oxo of the cubane. The Fe^{III} centers in the cubane (Fe_c) have pseudo-octahedral geometries composed

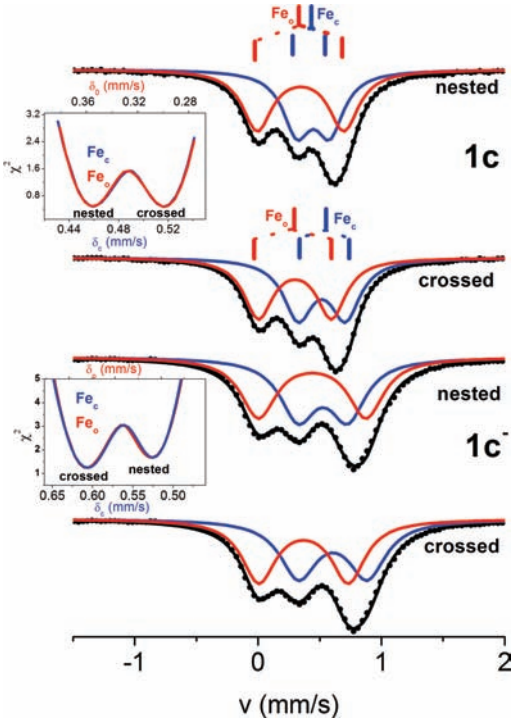

Figure 2. Zero field ^{57}Fe Mössbauer spectra of **1c** and **1c**$^-$ (black).[11c] Solid lines are theoretical simulations assuming two different iron sites (red and blue) at a 1:1 ratio. Insets are the dependence of the error parameter χ^2 of the fitting procedure of the experimental Mössbauer spectra of **1c** and **1c**$^-$ on the isomer shifts for the two different sites. During the fitting process, the ratio of the two sites was kept constant at 1:1.

of a *facial* array of three oxides and three nitrogens from the bridging pyrazolates. Given that the likeliest role for these clusters in nature is in electron transport, their redox properties are clearly critical. We have shown in preliminary cyclic voltammetric studies that the clusters are stable over five oxidation states, meaning that, at least in principle, they could be even more versatile electron transfer agents than their sulfur analogues. Moreover, the $E_{1/2}$ values across the manifold of four reduction steps are sensitive to variations in both R and X groups, making them an ideal platform for stabilizing and characterizing the partially reduced derivatives using spectroscopic methods.[11b,c] Of particular interest in this regard is the location (Fe_c or Fe_o?) and nature (localized, partially, or fully delocalized?) of the redox event. An answer to this question will rely heavily on the interpretation of redox-induced shifts in the various parameters obtained from Mössbauer, UV/vis/NIR, and X-ray photoelectron (XPS) spectroscopies.

One of our primary goals is to use this Fe_8 framework to provide a spectroscopic fingerprint that will aid in the future recognition of Fe_4O_4 cubanes in proteins, should they be isolated. In an earlier communication, we reported Mössbauer spectra for the archetype, **1a** and also **1c** (Figure 2), which show only three distinct peaks rather than the four anticipated for two distinct iron sites (two quadrupole doublets), indicating that the two peaks overlap. Two other octanuclear Fe_8 complexes containing $Fe_8(\mu_4\text{-}O)_4$ cores similar to that of the pyrazolato complexes discussed here are known, but no Mössbauer data have been reported in either case.[12] The spectra of **1a** and

(7) Laskowski, E. J.; Frankel, R. B.; Gillum, W. O.; Papaefthymiou, G. C.; Renaud, J.; Ibers, J. A.; Holm, R. H. *J. Am. Chem. Soc.* **1978**, *100*, 5322.

(8) (a) Vincent, J. B.; Olivier-Lilley, G. L.; Averill, B. A. *Chem. Rev.* **1990**, *90*, 1447. (b) He, C.; Mishina, Y. *Curr. Opin. Chem. Biol.* **2004**, *8*, 201.

(9) Fank, P.; De Tomaso, A.; Hedman, B.; Hodgson, K. O. *Inorg. Chem.* **2006**, *45*, 3920.

(10) Turano, P.; Lalli, D.; Felli, I. C.; Theil, E. C.; Bertini, I. *Proc. Nat. Acad. Sci.* **2010**, *107*, 545.

(11) (a) Raptis, R. G.; Georgakaki, I. P.; Hockless, D. C. R. *Angew. Chem., Int. Ed.* **1999**, *38*, 1632. (b) Baran, P.; Boca, R.; Chakraborty, I.; Giapintzakis, J.; Herchel, R.; Huang, Q.; McGrady., J. E.; Raptis, R. G.; Sanakis, Y.; Simopoulos, A. *Inorg. Chem.* **2008**, *47*, 645. (c) Chakraborty, I.; Baran, P.; Sanakis, Y.; Simopoulos, A.; Fachini, E.; Raptis, R. G. *Inorg. Chem.* **2008**, *47*, 11734.

(12) (a) Hahn, F. E.; Jocher, C.; Lugger, T. *Z. Naturforsch.* **2004**, *59b*, 855. (b) Gass, I. A.; Milios, C. J.; Whittaker, A. G.; Fabiani, F. P. A.; Parsons, S.; Murrie, M.; Perlepes, S. P.; Brechin, E. K. *Inorg. Chem.* **2006**, *45*, 5281.

1c can be deconvoluted into two overlapping doublets,[11b,c] but this deconvolution can, in principle, be carried out assuming either a nested model, where one quadrupole doublet lies entirely inside the second, or a crossed model, where the two doublets ride on each other (Figure 2). The dependence of the error parameter χ^2 of the fitting procedure for the isomer shifts for the two different sites is shown in the inset of Figure 2. The double-well structure shows that the nested and crossed models provide fits of almost identical quality ($\chi^2 = 0.5$), as a result of which it is not possible to distinguish between the two. However, the parameters that emerge are very different: the crossed model inevitably yields a much larger difference in isomer shifts for the Fe_c and Fe_o centers (0.52 and 0.30 mm/s, respectively) compared to the nested model (0.46 and 0.36 mm/s).

In the absence of a clear distinction between nested and crossed models based solely on the quality of the fit, we resorted to literature precedents to distinguish between the two possibilities. The trigonal bipyramidal geometry is, however, a rather uncommon motif for Fe^{III},[13] and the dearth of Mössbauer parameters for such centers makes direct analogues difficult to identify.[14] Nevertheless, the dependence of the isomer shift on coordination number has long been appreciated:[15] while it might be anticipated that an increase in the coordination number would result in a decrease of isomer shift due to higher covalency, this is generally more than offset by the accompanying increase in metal−ligand distances, and the isomer shift typically increases with increasing coordination number.[16] The magnitude of the quadrupole splitting, ΔE_Q, is related to the asymmetry of the metal coordination environment, and so, we anticipate that the trigonal bipyramidal coordination of the outer irons, Fe_o, should lead to larger values than the pseudo-octahedral geometry of the Fe_c sites. Unfortunately, both nested and crossed models are consistent with this expectation, and therefore, a safe distinction between the two possibilities cannot be made based solely on these arguments.[11b]

Ultimately, we aim to use the Mössbauer parameters to explore the nature of the mixed valency in reduced species such as $[Fe_8(\mu_4\text{-}O)_4(\mu\text{-}4\text{-}Cl\text{-}pz)_{12}Cl_4]^-$, a formally $Fe^{III}{}_7Fe^{II}$ species. The Mössbauer spectrum of this species again features an overlapping pair of quadrupole doublets (Figure 2), superficially very similar to the all-ferric cluster, and both nested and crossed models again give reasonable fits to the data. In this case, χ^2 is lower for the crossed model (Figure 2, inset). Although this suggests that the crossed model is more appropriate for **1c**$^-$, the difference is marginal and we feel that stronger evidence is required for secure assignment. The correct choice of model is absolutely critical as the nested and crossed variants lead to dramatically different conclusions regarding the nature of the mixed valency: if the nested model persists in the reduced species, then the parameters for the outer iron centers change to the largest extent, although distinct shifts are apparent in the cubane core as well, suggesting a more delocalized redox event. If, in contrast, a crossed model is adopted, then it is the parameters for the inner irons that change most dramatically, implying a cubane-localized redox event. The first of these possibilities appears to be inconsistent with XPS data that indicate delocalization in the core, and on this basis, we tentatively proposed that the crossed rather than nested model was appropriate for the singly reduced species.[11c]

The discussion in the preceding paragraphs illustrates the critical importance of the integrity of the assignment of the peaks in the Mössbauer spectrum to nested or crossed models. In both the all-ferric and the mixed valence cases, it proved impossible to distinguish the two alternatives based solely on the quality of the fit to the data, forcing us to rely on literature precedent or cross-reference to other spectroscopic signatures. In this paper, we report our efforts to establish a definitive assignment for the Mössbauer spectra by expanding the range of clusters sharing the $Fe_8(\mu_4\text{-}O)_4$ core and comparing the parameters obtained from nested and crossed fits to the corresponding data computed using density functional theory. We include examples where the terminal ligand, X, can be any of Cl, Br, or NCS (labeled **1**, **2**, and **3**, respectively) and the substituent R in the 4 position of the pyrazolate ring can be H, Me, or Cl (labeled **a**, **b**, and **c**, respectively). The structures with X = Cl; R = H (**1a**), X = Cl; R = Me (**1b**), X = Cl; R = Cl (**1c**) and X = Br; R = H (**2a**), have been reported previously, as have the Mössbauer spectra of **1a** and **1c**. We report here the synthesis, structure, and Mössbauer spectroscopy of the two further clusters, X = NCS; R = H (**3a**) and X = NCS; R = Cl (**3c**). These new experimental data are complemented by a series of calculations performed using density functional theory (DFT), where we compute both δ and ΔE_Q for all six of the Fe_8 clusters listed above. A number of authors have established an excellent correlation between computed and measured Mössbauer parameters for both mononuclear[17] and

(13) Lanznaster, M.; Hratchian, H. P.; Heeg, M. J.; Hryhorczuk, L. M.; McGarvey, B. R.; Schlegel, H. B.; Verani, C. N. *Inorg. Chem.* **2006**, *45*, 955.

(14) For example: (a) Fuchs, M. G. G.; Dechert, S.; Demeshko, S.; Ryde, U.; Meyer, F. *Inorg. Chem.* **2010**, *49*, 5853. (b) Lee, Y.; Mankad, N. P.; Peters, J. C. *Nat. Chem.* **2010**, *2*, 558. (c) Abbas, G.; Lan, Y.; Mereacre, V.; Wernsdorfer, W.; Clerac, R.; Buth, G.; Sougrati, M. T.; Grandjean, F.; Long, G. J.; Anson, C. E.; Powell, A. K. *Inorg. Chem.* **2009**, *48*, 9345.

(15) (a) Vrajmasu, V.; Münk, E.; Bominaar, E. *Inorg. Chem.* **2003**, *42*, 5974. (b) Greenwood, N. N.; Gibb, T. C. *Mössbauer Spectroscopy*; Chapman and Hall Ltd: London, 1971.

(16) (a) Liu, T.; Xia, B. H.; Zheng, Q. C.; Zhou, X.; Pan, Q, J.; Zhang, H. X. *J. Comput. Chem.* **2009**, *31*, 628. (b) Jaeger, T. D.; Van Heijnsbergen, D.; Klippenstein, S. J.; von Helden, G.; Meijer, G.; Duncan, M. A. *J. Am. Chem. Soc.* **2004**, *126*, 10981. (c) Barolo, C.; Nazeeruddin, M. K.; Fantacci, S.; Di Censo, D.; Comte, P.; Liska, P.; Viscardi, G.; Quagliotto, P.; Angelis, F. D.; Ito, S.; Gratzel, M. *Inorg. Chem.* **2006**, *45*, 4642. (d) Liu, I. P. C.; Chen, C. F.; Hua, S. A.; Chen, C. H.; Wang, H. T.; Lee, G. H.; Peng, S. M. *Dalton. Trans.* **2009**, 3571.

(17) (a) Bläs, R.; Guillin, J.; Bominaar, E. L.; Grodzicki, M.; Marathe, V. R.; Trautwein, A. X. *J. Phys. B: At. Mol. Phys.* **1987**, *20*, 5627. (b) Paulsen, H.; Kröckel, M.; Grodzicki, M.; Bill, E.; Trautwein, A. X.; Leigh, G. J.; Silver, J. *Inorg. Chem.* **1995**, *34*, 6244. (c) Lougear, A.; Grodzicki, M.; Bertoldi, C.; Trautwein, A. X.; Steiner, K.; Amthauer, G. *Phys. Chem. Miner.* **1999**, *27*, 258. (d) Zhang, Y.; Mao, J.; Oldfield, E. *J. Am. Chem. Soc.* **2002**, *124*, 7829. (e) Lovell, T.; Han, W. G.; Liu, T.; Noodleman, L. *J. Am. Chem. Soc.* **2002**, *124*, 5890. (f) Nemykin, V. N.; Kobayashi, N.; Chernii, V. Y.; Belsky, V. K. *Eur. J. Inorg. Chem.* **2001**, *3*, 733. (g) Filatov, M. *J. Chem. Phys.* **2007**, *127*, 084101. (h) Sinnecker, S.; Slep, L. D; Bill, E.; Neese, F. *Inorg. Chem.* **2005**, *44*, 2245. (i) Han, W.-H.; Liu, T.; Lovell, T.; Noodleman, L. *J. Comput. Chem.* **2006**, *27*, 1292. (j) Han, W.-H.; Noodleman, L. *Inorg. Chim. Acta* **2008**, *361*, 973. (k) Nemykin, V. N.; Kobayashi, K.; Chernii, V. Y.; Belsky, V. K. *Eur. J. Inorg. Chem.* **2001**, 733. (l) Zhang, Y.; Mao, J.; Oldfield, E. *J. Am. Chem. Soc.* **2002**, *124*, 7829. (m) Havlin, R.; Godbout, N.; Salzmann, R.; Wojdelski, M.; Arnold, W.; Schulz, C. E.; Oldfield, E. *J. Am. Chem. Soc.* **1998**, *120*, 3144. (n) Grodzicki, M.; Flint, H.; Winkler, H.; Walker, F. A.; Trautwein, A. X. *J. Phys. Chem. A* **1997**, *101*, 4202. (o) Zhang, Y.; Gossman, W.; Oldfield, E. *J. Am. Chem. Soc.* **2003**, *125*, 16387. (p) Praneeth, V. K. K.; Neese, F.; Lehnert, N. *Inorg. Chem.* **2005**, *44*, 2570. (q) Zhang, Y.; Oldfield, E. *J. Am. Chem. Soc.* **2004**, *126*, 9494. (r) Li, M.; Bonnet, D.; Bill, E.; Neese, F.; Weyhermuller, T.; Blum, N.; Sellmann, D.; Wieghardt, K. *Inorg. Chem.* **2002**, *41*, 3444. (s) García Serres, R.; Grapperhaus, C. A.; Bothe, E.; Bill, E.; Weyhermüller, T.; Neese, F.; Wieghardt, K. *J. Am. Chem. Soc.* **2004**, *126*, 5138.

Table 1. Selected Bond Lengths (Å) for Clusters **1a**,[a] **1b**,[a] **1c**,[a] **1c**$^-$,[b] **2a**,[a] **3a**, and **3c**

bond	**1a** (X = Cl)	**1b** (X = Cl)	**1c** (X = Cl)	**1c**$^-$ (X = Cl)	**2a** (X = Br)	**3a** (X = NCS)	**3c** (X = NCS)
Fe_c−O	2.032(6)−2.066(7)	2.028(5)−2.066(5)	2.047(2)	2.039(2)−2.050(2)	2.033(6)−2.060(6)	2.029(4)−2.058(3)	2.031(4)−2.055(4)
Fe_p−O	1.940(7)−1.960(6)	1.950(5)−1.970(5)	1.930(4)	1.919(2)−1.931(2)	1.943(6)−1.954(6)	1.938(2)−1.941(2)	1.934(4)−1.958(4)
Fe_c−N	2.044(9)−2.086(8)	2.044(7)−2.080(7)	2.101(3)	2.086(3)−2.103(3)	2.048(9)−2.090(8)	2.054(5)−2.085(4)	2.058(6)−2.077(6)
Fe_p−N	2.003(9)−2.038(10)	2.002(7)−2.034(6)	2.028(3)	2.012(3)−2.043(3)	2.008(9)−2.048(9)	2.016(6)−2.038(5)	2.006(6)−2.038(6)
Fe_p−X	2.271(4)−2.274(4)	2.284(2)−2.291(2)	2.293(2)	2.279(1)−2.299(1)	2.421(2)−2.425(2)	1.977(4)−1.996(4)	1.935(7)−1.964(6)

[a] Ref 11b. [b] Ref 11c.

polymetallic[15a,18] iron complexes across a wide range of oxidation states and coordination environments. Thus, we anticipate that only the correct model (nested or crossed) for the experimental data will provide a satisfactory correlation with the computed parameters.

Results and Discussion

The synthesis of complexes $[Fe_8(\mu_4\text{-}O)_4(\mu\text{-}pz)_{12}Cl_4]$ (**1a**), $[Fe_8(\mu_4\text{-}O)_4(\mu\text{-}4\text{-}Me\text{-}pz)_{12}Cl_4]$ (**1b**), $[Fe_8(\mu_4\text{-}O)_4(\mu\text{-}4\text{-}Cl\text{-}pz)_{12}Cl_4]$ (**1c**), and $[Fe_8(\mu_4\text{-}O)_4(\mu\text{-}pz)_{12}Br_4]$ (**2a**) by the reaction of anhydrous FeX_3 (X = Cl, Br) and the appropriate pyrazole ligand in the presence of a base has been reported previously.[11b] The NCS-capped species (**3a** and **3c**) were prepared from the corresponding chlorides, **1a** and **1c**, by a metathetical reaction using an excess of NH_4NCS in a CH_2Cl_2 solution. Satisfactory elemental analyses were obtained for all samples used in the Mössbauer experiments.

$$8FeX_3 + 12(4\text{-R-pzH}) + 20(Et_3N) + 4H_2O \rightarrow [Fe_8(\mu_4\text{-}O)_4(\mu\text{-}4\text{-R-pz})_{12}X_4] + 20Et_3NHX$$

$$X = Cl(\mathbf{1}), Br(\mathbf{2}) \quad R = H(\mathbf{a}), Me(\mathbf{b}), Cl(\mathbf{c})$$

$$[Fe_8(\mu_4\text{-}O)_4(\mu\text{-}4\text{-R-pz})_{12}Cl_4] + (\text{excess})NH_4NCS \rightarrow [Fe_8(\mu_4\text{-}O)_4(\mu\text{-}4\text{-R-pz})_{12}(NCS)_4](\mathbf{3})$$

Crystallographic Description. Important bond lengths and angles for **3a** and **3c** are summarized in Table 1, together with the corresponding data for previously published **1a**, **1b**, **1c**, and **2a** for comparison. All six $[Fe_8]$ complexes in the series share the same T−symmetric structural motif with a $Fe_8(\mu_4\text{-}O)$ core supported by 12 4-R-pz ligands, forming Fe_c−(μ-4-R-pz)−Fe_o bridges, and four terminal X ligands. The Fe_c−O and Fe_c−N distances are approximately 0.05−0.1 Å longer than their Fe_o−O and Fe_o−N counterparts, reflecting the higher coordination number of the former. With the obvious exception of the Fe_o−X distances, there are only very minor variations in bond lengths and angles across the entire series.

Mössbauer Spectroscopy. The Mössbauer spectra of complexes **1a**, **1b**, **1c**, **2a**, **3a**, and **3c**, all recorded at 78 K, are presented in Figure 3; the spectra of **1a** and **1c** have been presented in earlier reports.[11b,c] Fitted Mössbauer parameters, δ and ΔE_Q, for all six complexes are collected in Table 2. As was the case for the previously reported spectra of **1a** and **1c**, the spectra consist of three lines attributed to an overlapping pair of quadrupole doublets arising from the two distinct Fe^{III} centers. The only exception in this regard is **3c**, where the feature at high velocity splits at approximately +0.8 mm/s, allowing the identification of four distinct peaks: the similar intensities of the outer and the inner pair confirm unambiguously the nested model in this case. In the remaining five cases, however, deconvolution using nested or crossed models again yields fits of identical quality (Figure 3), leaving the correct choice of model unresolved. In both models, the isomer shifts, δ_o and δ_c, for the outer and cubane sites, respectively, fall in a narrow range (nested model: $0.36 \le \delta_o \le 0.40$ mm/s, $\delta_{o,av}$ = 0.38 mm/s, estimated standard deviation σ = 0.02 mm/s; $0.44 \le \delta_c \le 0.47$ mm/s, $\delta_{c,av}$ = 0.46 mm/s, σ = 0.01 mm/s. crossed model: $0.29 \le \delta_o \le 0.34$ mm/s, $\delta_{o,av}$ = 0.32 mm/s, σ = 0.02 mm/s; $0.48 \le \delta_c \le 0.54$ mm/s, $\delta_{c,av}$ = 0.51 mm/s, σ = 0.02 mm/s). The range of isomer shifts for the two types of iron center is comparable to the uncertainties in the experimental measurements (±0.01 mm/s), indicating that

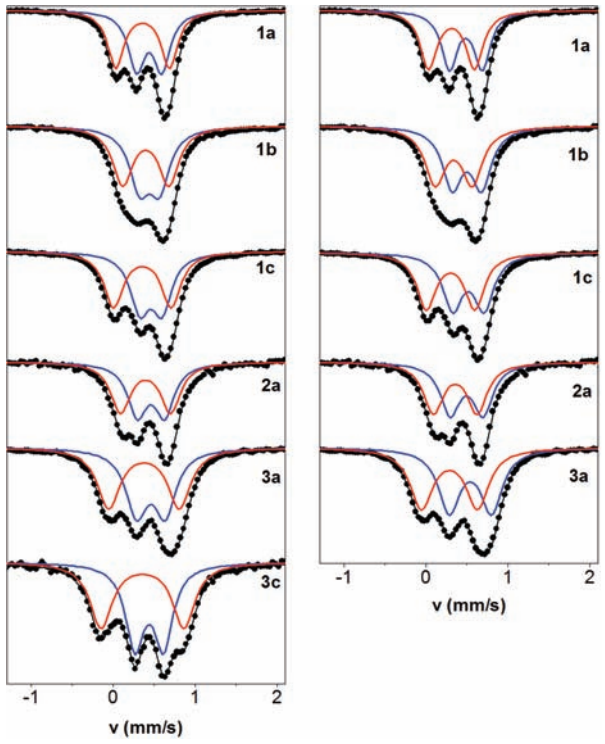

Figure 3. Zero field ^{57}Fe−Mössbauer spectra of complexes **1a**, **1b**, **1c**, **2a**, **3a**, and **3c** measured at 78 K. Fitting according to the nested (left) and crossed model (right) for cubane (blue) and outer (red) irons.

(18) (a) Hopmann, K. H.; Ghosh, A.; Noodleman, L. *Inorg. Chem.* **2009**, *48*, 9155. (b) Hess, C. R.; Weyhermüller, T.; Bill, E.; Wieghardt, K. *Angew. Chem., Int. Ed.* **2009**, *48*, 3703. (c) Martinho, M.; Xue, G.; Fiedler, A. T.; Que, L., Jr.; Bominaar, E. L.; Münck, E. *J. Am. Chem. Soc.* **2009**, *131*, 5823. (d) Han, W.; Liu, T.; Lovell, T.; Noodleman, L. *J. Comput. Chem.* **2006**, *27*(12), 1292. (e) Shoji, M.; Saito, T.; Takeda, R.; Kitagawa, Y.; Kawakami, T.; Yamanaka, S.; Okumura, M.; Yamaguchi, K. *Chem. Phys. Lett.* **2007**, *446*, 228. (f) Liu, T.; Lovell, T.; Han, W.; Noodleman, L. *Inorg. Chem.* **2003**, *42*(17), 5244. (g) Varnek, V. A.; Kryuchkova, N. A.; Bushuev, M. B. *J. Struct. Chem.* **2006**, *47*(6), 1177. (h) Barone, G.; Mastalerz, R.; Reiher, M.; Lindh, R. *J. Phys. Chem. A* **2008**, *112*, 1666.

Table 2. Experimental and Calculated Values of δ and ΔE_Q (mm/s) for the two Fe^{III} Sites in Clusters **1a**−**c**, **2a**, and **3a,c**[a]

				1a	**1b**	**1c**	**2a**	**3a**	**3c**
expt	nested	Fe_c	δ	0.44	0.44	0.46	0.46	0.46	0.47
			ΔE_Q	−0.31	−0.24	−0.27	−0.33	−0.35	−0.35
		Fe_o	δ	0.36	0.40	0.36	0.40	0.38	0.38
			ΔE_Q	−0.65	−0.56	−0.70	−0.61	−0.86	−1.00
	crossed	Fe_c	δ	0.48	0.50	0.52	0.50	0.54	
			ΔE_Q	−0.40	−0.36	−0.47	−0.40	−0.51	
		Fe_o	δ	0.31	0.34	0.30	0.36	0.29	
			ΔE_Q	−0.56	−0.45	−0.49	−0.54	−0.68	
DFT		Fe_c	δ	0.39	0.39	0.43	0.39	0.38	0.40
			ΔE_Q	−0.33	−0.30	−0.26	−0.31	−0.32	−0.31
		Fe_o	δ	0.30	0.30	0.30	0.30	0.31	0.31
			ΔE_Q	−0.62	−0.47	−0.66	−0.55	−0.80	−1.09

[a] All computed ΔE_Q are negative. In the case of **1a**, analysis of Mössbauer spectra recorded at 4.2 K in the presence of external magnetic fields indicated that $\Delta E_Q < 0$.[11b] Experimental data obtained by fitting to both the nested and crossed models are shown. The estimated standard deviation, σ, for all data listed is 0.01 mm/s

the isomer shifts are not affected in a statistically significant way by the variation of either the R or X groups, irrespective of the model adopted.

Computed values of the isomer shifts and quadrupole splittings for the broken-symmetry state (BS1 ($M_S = 0$), Scheme 1) of the all-ferric clusters **1a**, **1b**, **1c**, **2a**, **3a**, and **3c** are shown in Table 2. The corresponding values for the state of maximum multiplicity (HS ($M_S = 20$)), where all spin vectors are aligned parallel, are very similar and are collected in Table S2, Supporting Information. The calculated parameters (δ and ΔE_Q) are plotted against the experimental fits to the nested (red) and crossed (blue) models in Figure 4. The computed values of the isomer shift also reflect the effect of coordination number, with $\delta_c > \delta_o$, and fall into two rather narrow bands between 0.29 and 0.30 mm/s (Fe_o) ($\delta_{o,av} = 0.303$ mm/s, $\sigma = 0.005$ mm/s) and 0.38−0.43 (Fe_c) ($\delta_{c,av} = 0.397$ mm/s, $\sigma = 0.018$ mm/s). Given the uncertainty in the experimental data (±0.01 mm/s) and the fact that the error in calculated isomer shifts is typically of the order of 0.1 mm/s,[19] the correlations between experiment and theoretical isomer shifts within each class (Fe_c and Fe_o) are statistically meaningless. However, we anticipate that the differences in electron density, $\rho_0^S(0)$, between the two types of ferric site should be accurately modeled by the computational procedure and so, therefore, should the difference in isomer shifts $\Delta\delta_{co} = \delta_c - \delta_o = a[\rho_0^S(0)_o - \rho_0^S(0)_c]$. The computed densities yield $\Delta\delta_{co} = 0.094$ mm/s ($\sigma = 0.019$) which compares well with $\Delta\delta_{co} = 0.08$ mm/s ($\sigma = 0.02$ mm/s) obtained for the nested case but rather poorly with $\Delta\delta_{co} = 0.19$ mm/s ($\sigma = 0.03$ mm/s) for the crossed model. The computed isomer shifts, therefore, clearly support the nested model.

Whereas the isomer shifts of the two different iron sites for the six Fe_8 complexes examined here are not affected in a statistically significant way by the variation of either the R or X groups, the quadrupole splitting parameters prove to be quite sensitive to both R and X. The value of R^2 is much greater for the nested model (0.96) than the crossed alternative (0.59), and the former gives a gradient and intercept close to one and zero, respectively (0.96 and 0.04 vs 0.39 and 0.31 for the crossed model). Thus, our computed quadrupole splittings, like the isomer shifts, correlate strongly only with those obtained from the nested model, providing compelling evidence that this, rather than the crossed alternative, is appropriate for the description of the spectra of all six all-ferric clusters and not just **3c**, where the presence of two clearly resolved doublets provides an unambiguous assignment.

Mössbauer Spectra of the Reduced Species, 1c$^-$. With a secure assignment of the peaks in the all-ferric cluster in hand, we can now return to the singly reduced species and re-evaluate our earlier interpretation[11c] of the Mössbauer spectrum, shown in Figure 2. We have emphasized earlier that both nested and crossed models gave acceptable fits to the data for both oxidized and reduced species; the resulting parameters, δ and ΔE_Q, are collected in Table 3. The nested model for the all-ferric case has been verified above, but the choice of model for the mixed-valence species remains unresolved and has significant implications for our model of mixed valency. If the nested model is correct for both redox states, then the substantial changes in Mössbauer parameters for both Fe_c and Fe_o suggest that the redox event is delocalized over the entire Fe_8 framework. If, in contrast, the crossed model is valid then only the parameters for the Fe_c centers shift significantly, suggesting that the redox event is localized in the cubane core. We have previously adopted the crossed model as it appeared more consistent with XPS data, which indicates a cubane-based reduction. The multiplicity of the ground state of **1c**$^-$ was determined using X-band electron paramagnetic resonance (EPR) spectroscopy. Figure 5 shows the 4.2 K spectrum (solid line) of a glass sample of **1c**$^-$ in dichloromethane. The spectrum from **1c** (dotted line) is also shown for comparison. While **1c** is EPR silent at 4.2 K (as expected for a singlet ground state), **1c**$^-$ exhibits a strong derivative feature at $g \sim 1.97$, with a peak to peak width $\Delta H_{pp} = 75$ G, consistent with an $S = 1/2$ state. The temperature dependence of this signal indicates that it arises from the ground state.

We have shown previously[11b] that the dominant exchange pathway in the all-ferric cluster is an antiferromagnetic one between the cubane and outer irons, and the broken-symmetry state BS1, therefore, provides a reasonable first order description of the ground-state electron density. Computation of the parameters of the singly reduced species using a single determinant methodology is more problematic because the distribution of the additional electron is, to a large extent, determined by the alignment of spin vectors on the irons. Thus, for example, in the all-ferric broken-symmetry state BS1 ($M_S = 0$) shown in Scheme 1, all the spin-α orbitals of the iron centers in the cubane core are occupied, as are the spin-β orbitals on the peripheral irons. Using this initial density, an additional electron (spin-α by construction) must, therefore, necessarily be localized on one or more of the outer irons in the resultant broken-symmetry BS1 ($M_S = 1/2$) state (Scheme 1). When the polarization of the initial electron density is inverted, it is possible to converge to an alternative, but physically identical, all-ferric broken symmetry state BS1′ ($M_S = 0$), where the spin-α and spin-β manifolds are reversed. Addition of an extra electron to this density generates a mixed-valent analogue BS1′ ($M_S = 1/2$) where reduction is necessarily localized on the cubane irons. Only in the HS ($M_S = 39/2$) state, where the coupling is ferromagnetic and the spin-β orbitals on all eight irons are vacant, is the additional electron free to delocalize

(19) Neese, F. *Coord. Chem. Rev.* **2009**, *253*, 526.

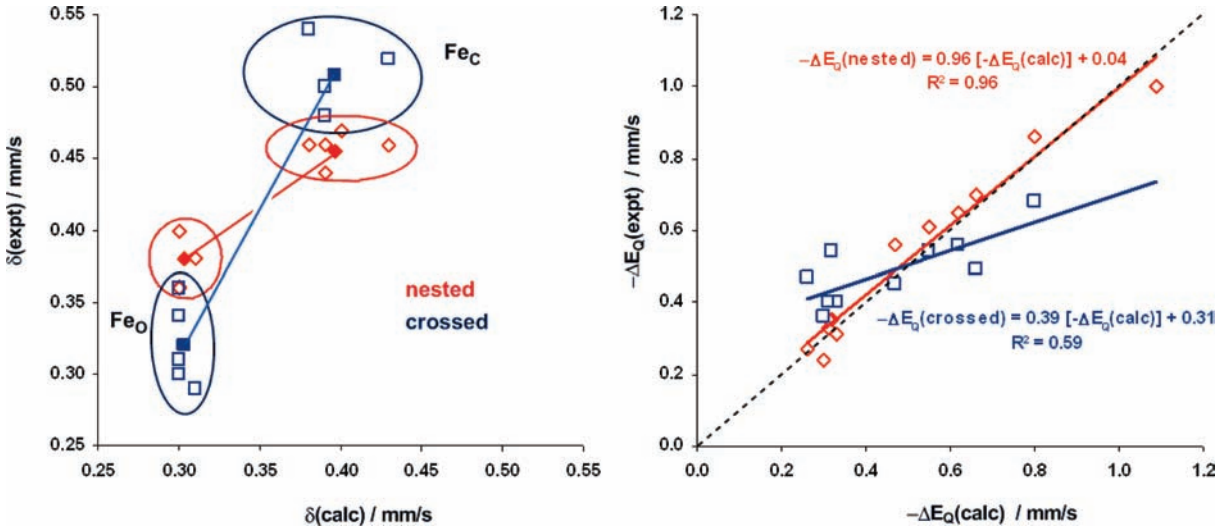

Figure 4. Correlation of ^{57}Fe Mössbauer parameters obtained from DFT with those from nested (red) and crossed (blue) fits to the experimental data. For the isomer shifts, the filled points represent the centers of gravity of the clusters of data points corresponding to Fe_c and Fe_o. The dashed black line for the ΔE_Q plot has a slope of 1.0 and intercept of 0.0.

Scheme 1. Alignment of Spin Vectors in the High-Spin (HS) and Broken-Symmetry (BS1 and BS1′) States of the All-Ferric (Fe^{III}_8) and Singly-Reduced ($Fe^{III}_7Fe^{II}$) Clusters

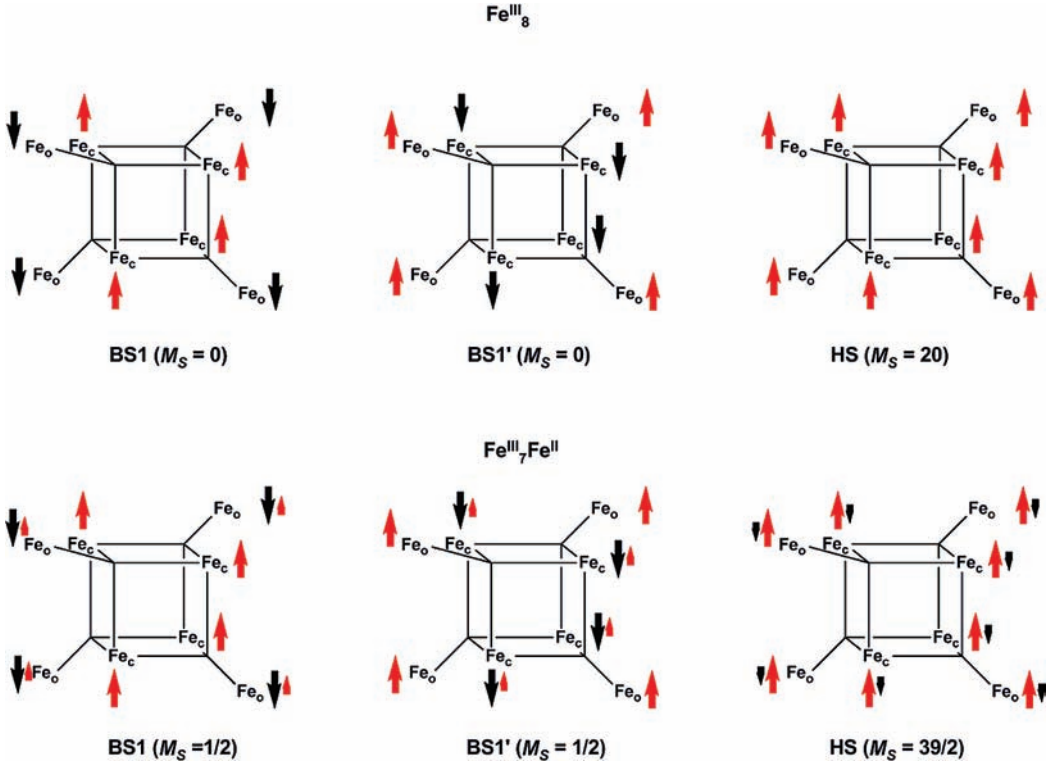

over the whole cluster. The relationship between the energies of the high-spin and broken-symmetry states and the true ground state of the mixed-valence species is a complex one, involving both Heisenberg and double exchange terms in the spin Hamiltonian.[20] However, in the present context where our interest centers on Mössbauer parameters that are determined largely by the (4s) electron density at the iron, we can take advantage of the localization imposed in the broken-symmetry states to explore how the Mössbauer parameters would vary in the (hypothetical) limits where the redox event is localized on the core (BS1′ (M_S = 1/2)) and on the periphery (BS1 (M_S = 1/2)). When the match between experiment and theory for HS (no restrictions) is compared, BS1 (reduction on outer irons) and BS1′ (reduction on cubane irons), we hope to validate (or refute) our adoption of the crossed model for the Mössbauer spectrum of the mixed-valent species with its implication of a cubane-based redox process.

Computed values for the three relevant states for $\mathbf{1c}^-$ are collected in Table 3, along with the spin densities. Data for the all-ferric cluster **1c** are also shown again for

(20) Clemente-Juan, J. M.; Borras-Almenar, J. J.; Coronado, E.; Palii, A. V.; Tsukerblat, B. S. *Inorg. Chem.* **2009**, *48*, 4557.

Table 3. Computed Values of δ, ΔE_Q (mm/s), and Spin Density for **1c** and Its One-Electron Reduced Counterpart, $\mathbf{1c}^{-}$[a]

			experiment			DFT					
			1c nested	$\mathbf{1c}^{-}$ nested[b]	$\mathbf{1c}^{-}$ crossed[b]	**1c** BS1 (M_S = 0)	$\mathbf{1c}^{-}$ BS1 (M_S = 1/2)	**1c** BS1′ (M_S = 0)	$\mathbf{1c}^{-}$ BS1′ (M_S = 1/2)	**1c** HS (M_S = 20)	$\mathbf{1c}^{-}$ HS (M_S = 39/2)
Mössbauer parameters	Fe_c	δ	0.46	0.51	0.59	0.43	0.43	0.43	0.52	0.42	0.50
		$\lvert\Delta E_Q\rvert$	0.27	0.40	0.56	−0.26	−0.36	−0.26	0.74	−0.17	0.69
	Fe_o	δ	0.36	0.44	0.35	0.30	0.40	0.30	0.31	0.30	0.31
		$\lvert\Delta E_Q\rvert$	0.70	0.87	0.73	−0.66	1.43	−0.66	−0.79	−0.69	−0.80
Mulliken spin densities	Fe_c					4.25	4.25	−4.25	−4.14	4.34	4.25
	Fe_o					−4.16	−4.05	4.16	4.17	4.22	4.22
	Cl									0.25	0.22

[a] Experimental data obtained from the nested fit (**1c**) and nested and crossed fits ($\mathbf{1c}^{-}$) obtained from ref 11c are shown for comparison. [b] The signs of the quadrupole splitting for $\mathbf{1c}^{-}$ are unknown, so only the magnitudes are shown.

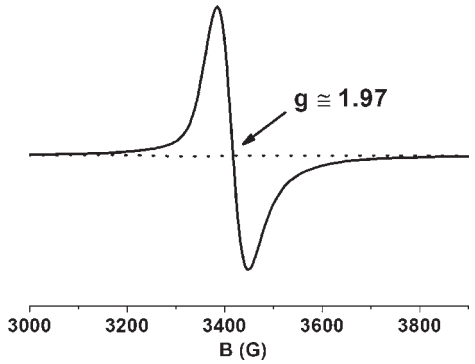

Figure 5. X-band EPR spectra of a dichloromethane glass of $\mathbf{1c}^{-}$ (solid line) and **1c** (dotted line) at 4.2 K; microwave power, 2.2 mW; modulation amplitude, 2.5 G_{pp}; microwave frequency, 9.41 GHz.

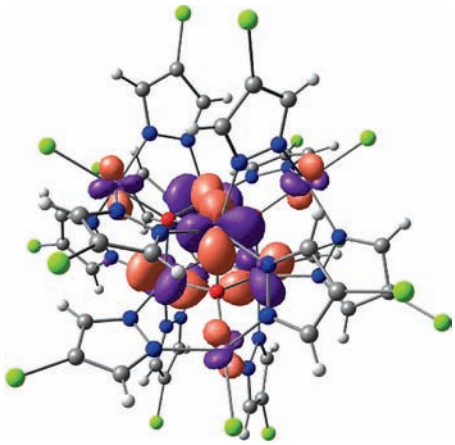

Figure 6. Highest occupied spin-β Kohn−Sham orbital in the HS (M_S = 39/2) state of $\mathbf{1c}^{-}$.

comparison. We emphasized above that there are no restrictions on the localization of the additional electron in the HS (M_S = 39/2) state because the spin-β components of the d orbitals on both core and outer irons are available. Nevertheless, the changes in spin density at self-consistency clearly indicate that the redox event is localized primarily on the cubane iron centers ($\Delta\rho Fe_c$ = −0.09 e^-, $\Delta\rho Fe_o$ = 0.00 e^-), while changes at the outer irons are minimal. There are, however, non-negligible changes in the spin density at the terminal chloride ligands, suggesting that the impact of the redox process extends to the covalency of the Fe_o−Cl bond. This partial delocalization is clearly reflected in the contour plot of the occupied spin-β Kohn−Sham orbital, which is indeed localized primarily on the cubane core but has significant delocalization tails on the outer iron centers (Figure 6). The changes in computed Mössbauer parameters are consistent with the changes in spin density: reduction to the HS (M_S = 39/2) state leads to a dramatic increase in both δ (0.42 to 0.50 mm/s) and ΔE_Q (−0.17 to 0.69 mm/s) for the Fe_c centers. The parameters for the peripheral irons, in contrast, are affected to a much lesser extent by the reduction ($\Delta\delta$ = 0.01 mm/s, $\Delta\Delta E_Q$ = −0.11 mm/s). These computed shifts are much more consistent with the crossed model than the nested alternative: most conspicuously, only the former replicates the invariance of the parameters for Fe_o as well as the significant increase in ΔE_Q for the cubane irons. On this basis, we conclude that the crossed model yields parameters that are fully consistent with the changes predicted for a redox event, where the additional electron is primarily localized within the cubane core, but with distinct delocalization tails on the outer iron centers.

The computed parameters for the two broken-symmetry states corroborate our view that the Mössbauer data are inconsistent with a redox event localized on the outer irons. Thus, in BS1 (M_S = 1/2), where the reduction is localized by construction on the outer irons, we see dramatic increases in the computed values of both δ and ΔE_Q. In fact, the unpaired electron is localized over only two of the four outer irons, and δ and ΔE_Q for these centers increase to ∼0.5 and ∼+2.1 mm/s, respectively while the other two remain almost unchanged (∼0.30, ∼−0.72). This should lead to the appearance of three distinct quadrupole doublets in the spectrum (in a 2:1:1 intensity ratio), a prediction that is clearly inconsistent with the experimental data. Even if the parameters for the four outer iron centers are averaged, the predicted changes are inconsistent with either nested or crossed models. Given that the self-consistent electron density in the HS (M_S = 39/2) state indicates that the excess β-spin is localized almost entirely on the cubane irons, it is unsurprising that the parameters for the BS1′ (M_S = 1/2) state, where the additional electron is on the cubane by construction, are very similar. Indeed, the two sets of parameters are equally consistent with experiment, and so, while the crossed model clearly indicates a primarily cubane-based redox event, we are unable to discount the possibility that a small amount of electron density is delocalized onto the outer irons as shown in Figure 6.

Conclusion

A secure assignment of the Mössbauer parameters is critical to our ongoing effort to characterize and understand the nature of the mixed valency in reduced analogues of the all-ferric Fe_8 clusters. In this paper, we have expanded the family of all-ferric clusters of generic formula $[Fe_8(\mu_4\text{-}O)_4(\mu\text{-}4\text{-}R\text{-}pz)_{12}X_4]$ to include the members with X = NCS and R = H and Cl. Structural characterization reveals little variation within the $Fe_8(\mu_4\text{-}O)_4$ cores. The availability of a range of clusters with ligands (both terminal, X, and 4-R-pyrazolate) with rather different electronic properties provides a sensitive platform for probing the influence of substitution on the Mössbauer spectrum. Comparison with DFT-computed parameters suggests that the two quadrupole doublets from the structurally distinct iron centers (Fe_c and Fe_o) form a nested rather than crossed pair in the all-ferric clusters, the larger quadrupole splitting corresponding to the 5-coordinate Fe_o-atoms. Although superficially similar, the spectrum of the reduced species is better fit to a crossed model, where the isomer shift and quadrupole splitting of the cubane irons is greatly enhanced due to localization of the additional electron in the core.

Experimental Section

Reagents obtained from commercial sources ($FeCl_3$, $FeBr_3$, pyrazole, 4-methylpyrazole, and NEt_3) were used as received. Solvents were purified prior use. The ligands 4-chloropyrazole, 4-bromopyrazole, 4-iodopyrazole, and 4-ethylpyrazole were synthesized according to the literature procedures.[21] Infrared, ^{1}H NMR, and UV−vis spectra were recorded on a Nicolet FT-IR 6000, Bruker ADVANCE DRX-500, and Varian CARY 500 Scan, respectively.

Synthesis. Complexes $[Fe_8(\mu_4\text{-}O)_4(\mu\text{-}pz)_{12}Cl_4]$ (**1a**), $[Fe_8(\mu_4\text{-}O)_4(\mu\text{-}4\text{-}Me\text{-}pz)_{12}Cl_4]$ (**1b**), $[Fe_8(\mu_4\text{-}O)_4(\mu\text{-}4\text{-}Cl\text{-}pz)_{12}Cl_4]$ (**1c**), and $[Fe_8(\mu_4\text{-}O)_4(\mu\text{-}pz)_{12}Br_4]$ (**2a**) were prepared as previously reported.[11b]

$[Fe_8(\mu_4\text{-}O)_4(\mu\text{-}pz)_{12}(NCS)_4]$ (3a). A flask charged with 0.100 g of **1a**, 10 mL of CH_2Cl_2, and ∼50-fold excess of NH_4SCN was stirred overnight, and a gradual color change to dark pink took place. The reaction was filtered, and X-ray quality crystals were obtained by slow Et_2O diffusion into the CH_2Cl_2 filtrate. IR (KBr disk, cm^{-1}): ν = 2011 (s), 1491 (w), 1417 (w), 1363 (m), 1267 (m), 1168 (m), 1146 (w), 1046 (s), 764 (m), 614 (w), 559 (w), 476 (s).

$[Fe_8(\mu_4\text{-}O)_4(\mu\text{-}4\text{-}Cl\text{-}pz)_{12}(NCS)_4]$ (3c). A flask charged with 0.100 g of **1c**, 10 mL of CH_2Cl_2, and ∼50-fold excess of NH_4SCN was stirred overnight. A color change to a dark pink color was observed. The reaction was filtered, and X-ray quality crystals were obtained by slow Et_2O diffusion into the CH_2Cl_2 filtrate. IR (KBr disk, cm^{-1}): ν = 2000 (s), 1382 (m), 1355 (m), 1298 (s), 1190 (m), 1152 (w), 1042 (s), 994 (w), 967 (m), 850 (w), 608 (m), 473 (s).

X-ray Crystallography. X-ray diffraction data, taken from a single crystal mounted atop a glass fiber with a Siemens SMART 1K-CCD diffractometer (298 K, λ = 0.71073 Å), were collected on a Bruker AXS SMART 1K CCD, area detector with graphite monochromated Mo Kα radiation (λ = 0.71073 Å) at room temperature using the program SMART-NT and processed by SAINT-NT.[22,23] An empirical absorption correction was applied by the program SADABS. The structures were solved by direct methods and refined by full-matrix least-squares methods on F^2.[24] All nonhydrogen atoms were refined anisotropically. H-atoms were placed in calculated positions with their thermal parameters riding on those of their C-atoms. Crystallographic details for **3a** and **3c** are summarized in Table 4.

Table 4. Crystallographic Data for **3a** and **3c**

	3a·CH_2Cl_2	**3c**
formula	$C_{42}H_{40}Cl_4Fe_8N_{28}O_4S_4$	$C_{40}H_{24}Cl_{12}Fe_8N_{28}O_4S_4$
formula weight	1717.86	1961.31
temperature (K)	298(2)	298(2)
crystal system	monoclinic	monoclinic
space group	$P2_1/n$	$P2_1/n$
a (Å)	20.073(4)	13.528(3)
b (Å)	16.004(3)	22.157(4)
c (Å)	21.505(4)	27.626(6)
β (deg)	106.775(3)	99.49(3)
V (Å)	6614(2)	8167(3)
Z	4	4
$D_{(cal)}$ (g cm^{-3})	1.725	1.595
μ (mm^{-1})	2.053	1.927
crystal size (mm)	0.24 × 0.19 × 0.18	0.25 × 0.18 × 0.08
reflection collected/$2\theta_{max}$	50188/56.02	29650/55.04
unique reflections/ $I > 2\sigma(I)$	14824/9114	18580/8976
number of parameters/ restraints	811/0	865/0
R/R_w	0.0464/0.1014	0.0727/0.1787
F (000)	3440	3872
goodness of fit	1.003	0.790

Mössbauer Spectroscopy. Mössbauer measurements were recorded on a constant acceleration conventional spectrometer with a ^{57}Co (Rh matrix) source. Variable-temperature spectra were obtained using Oxford cryostats, operating at 4.2−300 K. Isomer shift values (δ) are quoted relative to iron foil at 293 K. Analysis of the experimental spectra were performed with the WMOSS software (SEE Co, Edina, Minnesota). The χ^2 parameter of the fitting is given by the relation:

$$\chi^2 = (N_{data} - N_{var})^{-1} \sum_{i=1,\,Ndata} \frac{(D_i - T_i)^2}{{\sigma_i}^2}$$

where the sum is over all the points of the spectra, D_i is the i^{th} experimental datum, T_i is the i^{th} theoretical point, σ_i is the estimate of the noise in D_i, N_{data} is the total number of data points, and N_{var} is the number of free variables. For the preparation of the error plots shown in the insets of Figure 2, the ratio between the ferric sites was constrained to 1 and the isomer shift of either δ_c or δ_o was kept constant.

EPR Spectroscopy. X-band EPR measurements were performed with dichloromethane solutions (∼1.0 mM) of **1c** and **1c**$^-$ with a Bruker ER 200D instrument equipped with an ESR-9 Oxford cryostat and an Anristsu microwave frequency counter.

Computational Details. DFT calculations were performed on **1a**, **1b**, **1c**, **2a**, **3a**, **3c**, and **1c**$^-$ with the ORCA program[25] using the crystallographically determined structural parameters. The B3LYP[26] functional was used in conjunction with the CP(PPP)

(21) Ehlert, M. K.; Rettig, S. J.; Storr, A.; Thompson, R. C.; Trotter, J. *Can. J. Chem.* **1991**, *69*, 432.
(22) *SMART-NT Software Reference Manual*, version 5.059; Bruker AXS, Inc.: Madison, WI, 1998.
(23) *SAINT+ Software Reference Manual*, version 6.02; Bruker AXS, Inc.; Madison, WI, 1999.
(24) (a) Sheldrick, G. M. *SHELXS-90, Program for the Solution of Crystal Structure*; University of Gottingen: Gottingen, Germany, 1986. (b) Sheldrick, G. M. *SHELXL-97, Program for the Refinement of Crystal Structure*; University of Gottingen, Göttingen, Germany, 1997. (c) *SHELXTL-NT Software Reference Manual*, version 5.1; Bruker AXS, Inc.: Madison, WI, 1998.
(25) Neese, F. *ORCA-an ab initio, Density Functional and Semiempirical Program Package*, 2.6−35; University of Bonn: Bonn, Germany, 2008.
(26) (a) Lee, C.; Yang, W.; Parr, R. G. *Phys. Rev. B* **1988**, *37*, 785. (b) Becke, A. D. *J. Chem. Phys.* **1992**, *96*, 2155. (c) Becke, A. D. *J. Chem. Phys.* **1992**, *97*, 9173. (d) Becke, A. D. *J. Chem. Phys.* **1993**, *98*, 5648.

basis set[27] for Fe and TZVP[28] for the remaining atoms. The broken symmetry configuration was obtained with the "Flip-Spin" approach in ORCA, and all calculations were performed with increased integration grids (Grid4) and tight SCF criteria. For the Fe ions, the overall integration accuracy was increased to 7.0.

The Mössbauer parameters, specifically isomer shift (δ) and the quadrupole splitting (ΔE_Q), of a given iron center are related to the electron density.[29] The isomer shift (δ) depends critically on the local environment of the Fe nucleus in the absorber and has been shown to be proportional to the electron density at the Fe nucleus (ρ_0):

$$\delta = \frac{4}{5}\pi Z S(Z) e_0{}^2 R^2 \left(\frac{\delta R}{R}\right)[\rho_0{}^A(0) - \rho_0{}^S(0)]$$

where Z is the nuclear charge of the Mössbauer absorber, $S(Z)$ is the relativistic correlation factor, e_0 is the elementary charge, R is one-half of the sum of the radii of the Mössbauer nucleus in the ground (R_g) and the excited states (R_e), δR is the difference of the two radii, $\rho_0{}^A(0)$ is the nonrelativistic electron density at the nucleus for the Mössbauer absorber, and $\rho_0{}^S(0)$ is the same quantity for a given standard. The above equation can be simplified to

$$\delta = a[\rho_0{}^A(0) - C] + b$$

and the constants a, b and C of this expression can be estimated by plotting calculated values of $\rho_0{}^A(0)$ versus experimental isomer shifts for a variety of Fe-based complexes. Neese and co-workers have established suitable fit parameters for Fe-based complexes using various DFT functionals,[30,31] and the values of $a = -0.366$, $b = 2.852$, and $C = 11\,810$ reported in reference 31 are adopted in this work. In the absence of magnetic interaction (i.e., zero external magnetic field), the effect of the electric quadrupole interaction in a Mössbauer nucleus with $I = 3/2$ in the excited state and $I = 1/2$ in the ground state gives rise to a doublet splitting, which can be expressed as

$$\Delta E_Q = \pm\frac{1}{2} e Q V_{zz} \left(1 + \frac{\eta^2}{3}\right)^{\frac{1}{2}}$$

where η is the asymmetry parameter of the electric field gradient tensor, $\eta = (V_{xx} - V_{yy}/V_{zz})$, V_{xx}, V_{yy}, and V_{zz}, are the principal components of the electric field gradient tensor, e is the electric charge, and $Q(^{57}\text{Fe})$ (the nuclear quadrupole moment) is taken as 0.16 barn. The principal components V_{ii} are defined as $|V_{zz}| \geq |V_{yy}| \geq V_{xx}|$, and the asymmetry parameter η, therefore, lies in the range $0 \leq \eta \leq 1$.

Acknowledgment. Financial support for this project at UPR and Oxford was received through the National Science Foundation/EPSRC−International Collaboration in Chemistry program, Grants CHE-0822600 and EP/G002789/1, respectively. D.M.P. and R.G.R. also acknowledge a National Science Foundation−Doctoral Dissertation Enhancement Program, Grant CHE-0827841. J.E.M. is grateful for the allocation of computational resources from the Oxford Supercomputing Centre. E.D. and Y.S. acknowledge the support of the IMS.

Supporting Information Available: ORTEP plots for **3a** and **3c** (S1), computed values of the isomer shifts and quadrupole splittings for the maximum multiplicity, HS, states (S2), and crystallographic information files for **3a** and **3c**. This material is available free of charge via the Internet at http://pubs.acs.org.

(27) Schaefer, A.; Horn, H.; Ahlrichs, R. *J. Chem. Phys.* **1992**, *97*, 2571.
(28) Schaefer, A.; Huber, C.; Ahlrichs, R. *J. Chem. Phys.* **1994**, *100*, 5829.
(29) (a) Long, G. J., Ed. *Mössbauer Spectroscopy Applied to Inorganic Chemistry*; Plenum Press: New York1984−1989, pp 1−3. (b) Solomon, E. I., Lever, A. B. P., Eds. *Inorganic Electronic Structure and Spectroscopy*; John Wiley & Sons: New York, 1999; Vol. *1*, pp 161−211.
(30) Neese, F. *Inorg. Chim. Acta* **2002**, *337*, 181.
(31) Römelt, M.; Ye, S.; Neese, F. *Inorg. Chem.* **2009**, *48*, 784.